# A direct fluorescent signal transducer embedded in a DNA aptamer paves the way for versatile metal-ion detection

# Journal Pre-proof

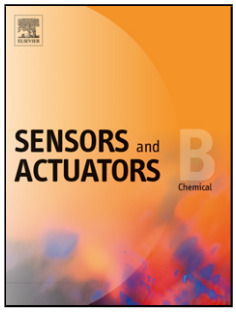


A direct fluorescent signal transducer embedded in a DNA aptamer paves the way for versatile metal-ion detection

Vlad-Stefan Raducanu, Fahad Rashid, Manal S. Zaher, Yanyan Li, Jasmeen S. Merzaban, Samir M. Hamdan

PII: S0925-4005(19)31575-8

DOI: https://doi.org/10.1016/j.snb.2019.127376

Reference: SNB 127376

To appear in: *Sensors and Actuators: B. Chemical*

Received Date: 9 July 2019

Revised Date: 23 October 2019

Accepted Date: 2 November 2019

Please cite this article as: Raducanu V-Stefan, Rashid F, Zaher MS, Li Y, Merzaban JS, Hamdan SM, A direct fluorescent signal transducer embedded in a DNA aptamer paves the way for versatile metal-ion detection, *Sensors and Actuators: B. Chemical* (2019), doi: https://doi.org/10.1016/j.snb.2019.127376

# A direct fluorescent signal transducer embedded in a DNA aptamer paves the way for versatile metal-ion detection

Vlad-Stefan Raducanu[1], Fahad Rashid[1], Manal S. Zaher[1], Yanyan Li, Jasmeen S. Merzaban, and Samir M. Hamdan*

King Abdullah University of Science and Technology, Division of Biological and Environmental Sciences and Engineering, Thuwal 23955, Saudi Arabia.

*****Corresponding author.
E-mail address: samir.hamdan@kaust.edu.sa (S.M. Hamdan)

**[1]**Contributed equally to this work.

**Highlights**

- We developed transducing technology that does not require external reporter
- We designed a DNA-based aptamer that directly transduces potassium ions concentration to fluorescence change
- Through G-rich sequence, the aptamer binds potassium ions and undergo conformational changes that can be sensed by cyanine dye
- The sensor detects potassium ions in the low micro-molar range with high selectivity against a wide range of ions including sodium

## Abstract

Using DNA aptamers as sensors for metal ions provide a variety of applications in biology and industry. Many of these sensors are based on guanine-rich DNA sequences that undergo conformational changes upon metal-ion binding. However, these sensors require an exogenous reporter that can recognize such DNA conformational changes and transduce the signal. Here, we bypass the exogenous reporter by embedding a signal transducer in the guanine-rich DNA aptamer that measures directly the DNA conformational changes upon metal-ion binding. Our signal transducer is an environmentally sensitive Cy3 fluorescent dye that is internally coupled to the DNA aptamer. We demonstrate the applicability of our embedded-signal transducer approach using a known potassium-responding aptamer. We next demonstrate the versatility of this approach by designing an aptamer sensor that can detect potassium ions in the low micro-molar range and with high selectivity against a wide range of ions including sodium. The aptamer accurately measured potassium ions concentration in a variety of aqueous and biological test samples. Our embedded-signal transducer approach will pave the way for the development of aptamer sensors for a variety of ligands.

**Keywords:** potassium sensor, DNA aptamer, G-quadruplex, metal ion detection, fluorescent signal transducer, Cy3 photoisomerization.

## 1. Introduction

The wide applications of biosensors in biomedicine, agriculture, environment and security have inspired significant research into the development of sensitive, selective, reliable and cost-effective biosensors. In particular, biosensors that detect metal ions gained popularity due to their ease of manipulation to detect wide range of ligands [1-3]. However, specificity toward target ligands and not toward other mono- and divalent metal ions remains difficult to achieve with biosensors [3, 4].

At the core of the biosensing technology are two elements: the biorecognition of an analyte and the transduction of this recognition into a quantifiable and measurable signal [3, 5]. The traditional use of proteins and enzymes for the biorecognition element has been replaced by the more versatile and cost-effective counterpart, DNA. The ability of DNA to bind a wide range of ligands and other small molecules makes it a rich resource for biosensors. In DNA-based biosensors, DNA aptamers and DNAzymes have been used as the ligand-recognition elements [6]. In DNA aptamers, the most common recognition mode is the formation of G-quadruplex structures in guanine-rich sequences upon metal ion binding, such as $K^+$, $NH_4^+$, $Na^+$, and $Pb^{2+}$ [1]. Recognition by DNAzymes, on the other hand, relies on their folding into a catalytically competent structure upon metal ion binding [3].

As for the transduction element, multiple methods have been used for signal readout, including those based on fluorescence, colorimetry, mass-sensitivity, electrochemistry, and chemiluminescence [2, 3]. Fluorescence-based methods are superior due to their high signal-to-noise ratios, requirement of minimal sample volume and ease of signal readout. One of the most popular fluorescence methods is Förster resonance energy transfer (FRET). Multiple studies have used FRET on DNA aptamers to sense structural changes in the DNA upon ligands binding [7, 8], including the use of FRET to detect $K^+$-induced G-quadruplex formation [9]. Despite FRET's popularity, it requires dual labeling and a change in distance between the donor and acceptor. This makes the development of FRET-based aptamers a very tedious task. A wealth of other fluorescence-based transducers has been developed [6, 8, 10-14]. However, all these methods require an indirect external dye as a transducer. This requirement increases the complexity of the assays and makes them unsuitable for applications in which a high dye concentration may interfere with the ligand or the medium. Additionally, the response to such external transducers depends on the binding of both the ligand to the sensor and the sensor to the transducer, each with its own affinity. This additive effect decreases the working range, as well as the sensitivity of the sensor. At the same time, the dependence of the assay on the concentration of the dye renders measurement reproducibility and error minimization challenging.

Recently, Umrao et al. [15] coupled a thrombin protein binding aptamer to a Cy3 fluorophore and showed that thrombin binding enhanced the fluorescence through protein-induced fluorescence enhancement (PIFE). This methodology eliminates the requirement of the dual labeling in FRET or the need for an indirect external signal transducer. However, the applicability of this methodology is restricted to systems where a protein is the ligand itself. In a recent work, we have characterized the modulation of PIFE in cyanine dyes, such as Cy3, within the context of cyanine dyes-conjugated DNA systems [16]. Here, we relied on this

characterization to develop a fluorescent transducing approach that extends the advantages of PIFE-based transduction to a protein-free aptamer system.

Our fluorescent-transducing approach takes advantage of the environmental sensitivity of cyanine dyes. These dyes exhibit interesting photophysical properties due to their non-rigid structures with a polymethine bond connecting two indole rings [17, 18]. The fluorescence of these dyes, as quantified by fluorescence emission intensity, fluorescence lifetime or quantum yield, depends on the cis-trans photoisomerization rate around their polymethine bond. This photoisomerization rate in turn hinges on the environment surrounding the fluorophore [16, 17]. Therefore, we conjectured that Cy3, when embedded in an aptamer, can report directly on the DNA conformational changes upon metal ion binding. In this study, we opted to characterize and develop this transducing approach with potassium ion as a ligand of choice. We showed, using an incorporated Cy3 to a well-established G-quadruplex potassium sensor, that Cy3 can directly transduce the signal from potassium binding. We then demonstrated that this transducing approach can be developed to produce a new DNA sensor for potassium detection with remarkable selectivity, affinity and environmental stability. Notably, this sensor was able to determine the equivalent $K^+$ concentration in several test samples. We envision that future investigations can apply the same general concepts to other ligands including nucleic acids or other small molecules.

## 2. Materials and Methods

### 2.1 Materials

DNA and RNA oligos O328 with an 18-nt long G-rich sequence (GAGGGACGGGGCAGGAGG) were custom synthesized unlabeled or labelled with Cy3 or Cy5 incorporated via phosphoramidite linkage at various positions. A DNA oligo G1 with a 21-nt long G-rich sequence (GGGTTAGGGTTAGGGTTAGGG) was custom synthesized labelled with Cy3 incorporated via phosphoramidite linkage at its 5' end. These oligos were synthesized and HPLC purified by Integrated DNA Technologies (IDT, Inc.). All salts used in this study are HPLC grade and were purchased from Sigma Aldrich. DNase-free water was used to dissolve all salts and/or DNA.

### 2.2 Time-Resolved Fluorescence Lifetime Measurements

The time-resolved fluorescence lifetimes of Cy3-O328 in increasing concentrations of KCl, NaCl and $NH_4Cl$ as well as 10 mM of various salts (LiCl, $MgCl_2$, $MnCl_2$, $CaCl_2$, CsCl, $ZnCl_2$ and $SrCl_2$) were measured using time-correlated single-photon counting (TCSPC) mode on a QuantaMaster 800 spectrofluorometer (Photon Technology International Inc.) equipped with a Fianuim supercontinuum fiber laser source (Fianium, Southampton, U.K.) operating at a 20-MHz repetition rate. The arrival time of each photon was measured with a Becker-Hickl SPC-130 time-correlated single photon counting module (Becker-Hickl GmbH, Berlin, Germany). Measurements were collected under magic-angle (54.7°) conditions and photons were counted using time-to-amplitude converter (TAC). To reduce the collection of scattered light, a longpass filter (550 nm) was placed on the emission side. In all measurements, 10,000 counts were

acquired. The instrument response function (IRF) was estimated using a Ludox colloidal silica suspension dissolved in water.

Cy3 was excited at 535 nm and the emission was collected at 565 nm with a 5-nm slit width for both excitation and emission. The amplitude-averaged lifetimes of Cy3 in all different cases were estimated by fitting lifetime decays to two exponentials using the FluoFit software package (PicoQuant) and applying the IRF. The best fit was chosen based on the reduced chi-square and randomness of the residuals. The lifetimes of Cy3-O328 in the presence of increasing concentrations of KCl, NaCl or $NH_4Cl$ were plotted against the dimensionless $\log_{10}$ of the respective salt concentrations normalized to 1 nM. The resulting curves were fit to the sigmoidal Hill 1 function in Origin (as described in Eq. 5) while fixing the initial fluorescence lifetime to that of a Cy3-O328 sample in water. The reported dissociation constants ($K_D$) are the actual dissociation constants of the respective salts from Cy3-O328 after back calculating the concentration from the fitted sigmoidal function. On the other hand, $n^*$ is the apparent Hill coefficient of the fit.

### 2.3 Steady-State Fluorescence

Steady-State Fluorescence spectra and intensities of Cy3-O328 were acquired at room temperature using a microplate spectrofluorometer (TECAN infinite M1000) in increasing concentrations of KCl. In both cases, Cy3 was excited at 535 nm ($\lambda_{max\text{-}ex}$). Full emission spectra were collected between 520 and 700 nm while the fixed-wavelength fluorescence intensity was only recorded at 565 nm ($\lambda_{max\text{-}em}$) for plotting the $K^+$-dependent response curve. Excitation and emission slit widths were set to 5 nm, and measurements were acquired with an integration time of 0.1 s. The emission spectra and intensities were corrected by subtracting the background emission of a water blank. The spectra were further smoothened using the fast Fourier transform (FFT) implemented in the Origin-pro software. The noise harmonics were determined at a dynamic window size of 5 nm corresponding to the slit width. The fluorescence intensities of Cy3 at different KCl concentrations were plotted against the dimensionless $\log_{10}$ of the KCl concentration normalized to 1 nM. This curve was fitted to the Hill 1 function similar to the lifetime response curve. The reported $K_D$ and $n^*$ are as described above for the time-resolved measurements. Error bars correspond to the variation in the measurement between two replicates.

### 2.4 Absorbance Measurements

The absorbance of Cy3-O328 in increasing concentrations of KCl was measured at room temperature using a microplate spectrophotometer (TECAN infinite M1000). The Cy3-O328 concentration was kept at 1 µM such that the absorbance was below 0.1 to minimize the reabsorption effect. The absorption spectra were acquired from 440 to 600 nm. Criteria of 1-nm wavelength step size along with 100 flashes per step were used. These spectra were corrected by measuring the instrumental baseline with a water blank. Similar to the emission spectra, the absorption spectra were smoothened using FFT. Absorbance was quantified by integrating over the entire spectra. Absorbance change due to increasing salt concentration was calculated as a percentage with respect to the absorbance of the zero-salt sample.

### 2.5 Circular Dichroism (CD) Measurements

The CD of unlabeled O328 in increasing concentrations of KCl was measured at room temperature using a CD spectrophotometer (JASCO J-1500). The unlabeled O328 concentration was kept at 20 μM to ensure a reliable signal-to-noise ratio. The CD spectra were acquired from 205 to 350 nm. Criteria of 1-nm wavelength step size along with 50 nm/min scanning speed were used. These spectra were corrected by subtracting the instrumental baseline with a water blank. Similar to the emission spectra, the CD spectra were smoothened using FFT. The total absorption was also simultaneously monitored with the CD to monitor the consistency of the oligo concentration.

### 2.6 Temperature Dependence Measurements

Steady-state fluorescence emission spectra of Cy3-O328 were acquired at different temperatures in 5 °C increments, using a FlouroMax-4 spectrofluorometer with an integrated sample holder for temperature control. For all temperatures, Cy3 was excited at 535 nm ($\lambda_{max\text{-}ex}$) and the emission spectra were collected between 550 and 700 nm and then integrated over this interval. Excitation and emission slit widths were set to 5 nm and measurements were acquired with an integration time of 0.2 s. Before integration, the emission spectra were corrected by subtracting the background emission spectra of a water blank. All the intensity values at different temperatures reflect the background subtraction and the spectral integration.

In case of the control Cy3-labeled oligonucleotides that don't form secondary structure, the temperature-dependence of the fluorescence emission intensity is described by Eq. (20) (Supplementary Methods). If the oligonucleotide has considerable secondary structure, the temperature-dependence of Cy3 photoisomerization will be convoluted with the temperature-dependence melting of the DNA secondary structure [19]. Moreover, if the secondary structure is induced by the biding of a certain ligand, the temperature-dependence curves will be also convoluted with the temperature-dependence of the binding dissociation constant via the van't Hoff equation [20, 21]. In the case of Cy3-O328, all three temperature-dependence mechanisms coexist. An analytical equation for the temperature-dependence curves can be constructed mathematically, but given the large number of free parameters involved in such an equation, it would be poorly constrained for fitting the experimental data. In order to simplify the fitting of the temperature-dependence curves of Cy3-O328 fluorescence emission intensity, we employed a Shape Language Modeling (SLM) toolkit implemented in MATLAB [22]. The experimental datapoints were fit to a piecewise linear model using SLM with variable number of knots. The interior knots were allowed to be free and no additional constraints were added to the model. Even though less informative than an analytical equation, the piecewise linear model allows for estimating an apparent value for the main parameters of interest of the temperature-dependence curves.

### 2.7 Preparation of the Test Samples

The potassium standards were purchased from Ricca Chemical. The bottled drinking water was purchased locally from randomly selected retail outlets. DNase-free water was used for all the

dilutions employed in the experiments for determining the potassium equivalent content of the test samples.

All the studies were performed in accordance with an approved protocol by the Institutional Animal Care and Use Committee at KAUST. During all the procedures, adult male mice were anesthetized with isoflurane inhalant (3-4% for induction and 1-3% for maintenance). Analgesia was confirmed by a toe pinch. For urine collection, the mice were restrained, held over a collection tube and lightly stroke on the belly. For blood collection, a "V" – shaped cut in the abdomen was made and the intestines were gently moved aside. The aorta abdominalis was identified, and a syringe with 23G needle was inserted cranially to collect blood from the aortaventralis. The whole blood samples were left to clot at 37 °C (water bath) for 30 minutes, and centrifuged at 2000x*g* for 10 minutes. The clear supernatant was collected as blood serum.

## 3. Results

### 3.1 Internal Cy3 fluorescence transduces metal ion-induced DNA conformational change

In a previous work [16], we characterized several factors that may influence the interactions of the DNA with Cy3 and alter its photoisomerization rate. Here, we explore the applications of this characterization in developing a fluorescent transducer that takes advantage of the environmental sensitivity of Cy3 photoisomerization. In particular, we hypothesized that if Cy3 is coupled to an aptamer that undergoes a ligand-induced conformational change, which in turn alters Cy3's photoisomerization rate, then Cy3 can transduce the signal into a measurable fluorescence change (Fig. 1A).

To test this hypothesis, we turned our attention to the well-established use of G-quadruplex aptamers as metal-ion biosensors [1, 7, 9, 11-14, 23-33]. G-quadruplexes are G-rich ssDNA sequences, which tend to fold into secondary structures that are stabilized in the presence of different metal ions, most notably $K^+$. In particular, we conjugated Cy3 through phosphoramidite linkage to a G-rich sequence (G1), which was previously reported to respond to $K^+$ binding [34-36]. The resulting conjugated system is therefore referred to as Cy3-G1. Upon $K^+$ binding, this DNA aptamer folds into a parallel/antiparallel-mixed G-quadruplex [34, 35]. Previously, this signal was transduced in the form of isothermal titration calorimetry (ITC) response [34], circular dichroism (CD) response [36], electrospray ionization mass spectrometry (ESI-MS) titration curves [35] and the distance dependence of dark quenching between a fluorophore and a dark fluorescence quencher [34]. In these previous studies, the reported linear response range to $K^+$ binding was between 20 μM and 1 mM, with a dissociation constant ($K_D$) of ~78 μM.

Throughout this study, we opted to incorporate the Cy3 fluorophore into the sugar-phosphate backbone through phosphoramidite rather than post-synthetic labeling via N-hydroxysuccinimide (NHS)–amine chemistry, because this approach provides Cy3 with greater sensitivity to the conformational changes in the DNA molecule to which the dye is attached [16]. To examine the ability of the embedded Cy3 in transducing the DNA conformational changes induced by $K^+$ binding into an aptamer, we measured the time-resolved fluorescence lifetime of Cy3-G1 upon increasing the concentration of $K^+$ in the form of KCl salt. At room temperature, KCl and $K^+$ concentrations in water are equivalent since KCl almost completely disassociates into its

constituent ions. Experimentally, measured fluorescence lifetime meets all the requirements of a physical observable for signal transducing from a population with two species, bound and unbound aptamers, as described in Supplementary Methods. Moreover, the measured fluorescence lifetime of a mixture of two populations with two different lifetimes and the same absorption and emission spectra is a linear combination of the concentration-weighted individual lifetimes [37]. Cy3-G1 showed a fluorescence lifetime of 1.90 ns in ultra-pure water, which continuously increased upon increasing the $K^+$ concentration and reached a saturation of 2.27 ns at ~10 mM (Fig. 1B). Importantly, the $K_D$ and the response range of Cy3-G1 to $K^+$ (Fig. 1B) is consistent with previous reports [34, 35].

### 3.2 Using Cy3 as an embedded transducer to build a potassium sensor from scratch

To ensure that our transducing technology is not G1-sequence specific, we explored its applicability and versatility in other DNA-Cy3 conjugated contexts. Therefore, we sought to develop another DNA aptamer for $K^+$ sensing keeping in line with our embedded Cy3 transducing element. In our recent work, we observed a $K^+$-induced hyper-fluorescence of a G-rich ssDNA sequence (O328) [16]. We hypothesized that the binding of $K^+$ to this ssDNA most likely induces the formation of a secondary structure. Hence, we carried out Circular dichroism (CD) measurements of an unlabeled O328 oligo. We observed a specific CD spectrum between 220 nm and 350 nm; this spectrum was shifted and amplified by the addition of KCl (Fig. 2A), while the total absorbance showed no change (Fig. 2A, inset). This experiment demonstrates that a $K^+$-induced secondary structure is being formed in O328. It is worth noting that this structural change is intramolecular rather than intermolecular as we confirmed through single molecule work [16]. Taken together, these results point towards the potential of O328 sequence to sense $K^+$.

To transduce this structural change into a fluorescence signal, we conjugated Cy3 through phosphoramidite linkage to this DNA sequence. Cy3 fluorescence and its modulation is highly sensitive to the overall structure of the DNA-Dye complex, which is influenced by the position of the fluorophore within the DNA, among other factors [16, 38, 39]. To maximize the signal readout of the $K^+$-induced fluorescence enhancement, we screened for several Cy3 positions in O328 (Fig. 2B). With the exception of Cy3 terminally conjugated to O328, $K^+$ binding induced a fluorescence enhancement with a maximum of ~55% when Cy3 was conjugated right in the middle of the oligo. We adopted this particular Cy3-O328 for further characterizations.

The time-resolved fluorescence lifetime decays of Cy3-O328 measured at increasing concentrations of $K^+$ (0 – 1 M) showed a continuous increase of Cy3 fluorescence in response to increasing $K^+$ concentration (Fig. 2C). These decays were fit to two-exponential decays yielding an amplitude-weighted average of fluorescence lifetimes. Cy3-O328 exhibited a fluorescence lifetime of 1.8 ns in ultra-pure water in the absence of any additional metal ions (Fig. 2D). This fluorescence lifetime continuously increased as the $K^+$ concentration increased, reaching a saturation of ~2.8 ns at ~10 mM KCl (Fig. 2D). This increase in Cy3 fluorescence lifetime indicates that the $K^+$-induced conformational change in the DNA acts locally in such a way that rigidifies Cy3, thus decreasing its photoisomerization rate and increasing its experimentally measured fluorescence lifetime.

We plotted the fluorescence lifetime values against the dimensionless $\log_{10}$ of the $K^+$ concentration (Fig. 2D). The data points seem to follow a sigmoidal response; hence, we fit the curve with Eq. (5) (Supplementary Methods) with a fixed $\tau_0$ value of 1.8 ns (the fluorescence lifetime at zero salt). This fit generated a maximum fluorescence lifetime of 2.83 ns at saturating $K^+$ concentration (Fig. 2D). These two parameters gave Cy3-O328 a dynamic range of ~1 ns. The fit of the binding kinetics resulted in a $K_D$ value of ~6 μM (3.77 in $\log_{10}$ scale), demonstrating that our Cy3-O328 aptamer is ultrasensitive to $K^+$ in the low micro-molar range. The apparent Hill coefficient ($n^*$) of this fit (~6) reflects the $\log_{10}$ transformation of the concentration axis and not the true Hill coefficient.

The time-resolved fluorescence lifetime measurements reported above were performed at fixed excitation and emission wavelengths. Such fixed-wavelength measurements do not discriminate between a true change in Cy3 fluorescence resulting from $K^+$-dependent secondary structure formation in the DNA and a spectral-chromatic change induced by the same structure formation. To probe the latter case, we acquired steady-state fluorescence emission spectra (520 – 700 nm) of Cy3-O328 at several $K^+$ concentrations (Fig. 2E). These emission spectra with increasing $K^+$ concentrations up to 1 M did not exhibit any significant spectral-chromatic change. Analogous to the lifetime measurements, the steady-state fluorescence intensities increased continuously as the $K^+$ concentration increased from zero to 1 mM. For a better comparison between the lifetime and steady-state measurements, we normalized their response curves and calculated the Pearson correlation coefficient in the quasi-linear response range in order to assess the agreement between the two measurements analytically (Fig. 2F). A Pearson correlation coefficient of ~0.98 indicated a strong agreement between the measurements. Moreover, absorbance measurements of Cy3-O328 under various $K^+$ concentrations did not exhibit any spectral-chromatic changes or major variations in their integrated values, confirming the absence of non-linear effects (Fig. S1A). We therefore concluded that the response curve can be reproduced by either approach.

Taken together, the ability of O328 to respond to $K^+$ ions by a DNA conformational change and the ability of Cy3 to transduce this response into a fluorescence change suggest that Cy3-O328 possess the two components of a biosensor. Moreover, Cy3-O328 $K^+$-response was in the low micro-molar range, indicating high sensitivity. Regarding Cy3-O328 as a sensor, we estimated the classical $EC_{10}$ and $EC_{90}$ values defined for sigmoidal response curves [40]. The sigmoidal response curve (Fig. 2D) showed an $EC_{10}$ of 440 nM (2.64 in $\log_{10}$ scale) and an $EC_{90}$ of 260 μM (5.41 in $\log_{10}$ scale) defining a working range that spans over 600 folds. This working range is transduced by Cy3 into 1-ns dynamic range of the fluorescence lifetime. Moreover, these $K^+$-induced structural changes are specific to DNA, because an oligo with the same sequence as O328 but in an RNA form was insensitive to the addition of KCl (Fig. S1B).

### 3.3 Properties of the response curve of the designed DNA sensor with embedded Cy3 transducer

To further evaluate the performance of Cy3-O328 as a sensor, we investigated the properties of its response curve in the interval between $EC_{10}$ and $EC_{90}$. In general, the performance of a sensor is assessed based on several factors including sensitivity, reproducibility, linearity and selectivity [41]. We started by investigating the local response over the whole concentration dependence; thus, we adopted the formalism of a local response coefficient for sigmoidal curves as described

earlier [42]. We changed the definition of the response coefficient function to reflect the dynamic range of our sensor's lifetime as shown in Eq. (9) (Supplementary Methods). The resulting curve (Fig. 3A) shows a single-peak function, with the peak centered at ~3 μM (3.45 in $\log_{10}$ scale), relatively comparable to the $K_D$ (6 μM). This suggests that the maximum sensitivity of the sensor is around the $K_D$. Between $EC_{10}$ and $EC_{90}$, our sensor offers a 2 to 9% local response to a variation in concentration (Fig. 3A). Considering the high temporal resolution of currently available time-resolved detectors, this response is significant. This local response coefficient indicates that if the concentration is varied by a certain percentage, the response will vary by that percentage multiplied by the local response coefficient of the initial concentration of the variance. For example, the local response coefficient would predict that doubling the concentration from 3 μM to 6 μM would result in 9% change in the fluorescence lifetime. This 9% change translates to ~200 ps, which is easily resolvable by a detector with 25-ps time resolution.

Next, we sought to verify the reproducibility of Cy3-O328; therefore, we determined a theoretical estimate of the uncertainty associated with sensing and transducing an unknown $K^+$ concentration using our Cy3-O328 sensor. The relative uncertainty is given by Eq. (15) (Supplementary Methods) and plotted in Fig. 3B. This relative uncertainty is dictated by the parameters of the response curve as well as the uncertainty of the lifetime measurement. The relative error varies between 15% and 55% in the interval between $EC_{10}$ and $EC_{90}$, assuming an uncertainty of the lifetime of 25 ps as dictated by the instrument's detector. The curve exhibits a single local minimum at around 3.8 μM (3.58 in $\log_{10}$ scale), in the vicinity of the $K_D$ (6 μM). This suggests that in the linear range around the $K_D$, error is minimized, and the measurements are highly reproducible.

We then moved to assessing the linearity of Cy3-O328. The response curve presented in Fig. 2D is very useful as a calibration curve. However, the inverse curve would be required for estimating unknown samples. Mathematically, this is possible if and only if the response curve is invertible, such that only one fluorescence lifetime corresponds to any given metal ion concentration. Then, the inverse function, described by Eq. (11) (Supplementary Methods) and plotted in Fig. 3C, takes a measured fluorescence lifetime of Cy3-O328 sensor in an unknown $K^+$-containing solution and outputs the corresponding $K^+$ concentration. This curve exhibits an almost linear relationship between $\log_{10}$ of the concentration (y-axis) and fluorescence lifetime (x-axis) in the interval between $EC_{10}$ and $EC_{90}$ (Fig. 3C). Furthermore, this curve defines the dynamic range of the fluorescence lifetime (1.9 – 2.7 ns) required for the Cy3-O328 sensor to operate in the interval between $EC_{10}$ and $EC_{90}$.

Secondary structures of DNA, especially G-quadruplexes, have been shown to coordinate multiple mono- and divalent metal ions [14]. Hence, we sought to investigate the ability of Cy3-O328 in coordinating metal ions other than $K^+$, including the physiologically relevant $Na^+$ ions. We measured the time-resolved fluorescence lifetime of Cy3-O328 in the absence and presence of 10 mM of various cations ($Li^+$, $Mg^{2+}$, $Mn^{2+}$, $Ca^{2+}$, $Cs^+$, $Zn^{2+}$, $Na^+$, $NH_4^+$, $K^+$ and $Sr^{2+}$) in the form of chloride salts (Fig. 3E). The chloride anion was maintained in all the tested salts such that we could assess the exclusive effect of the cations. In the presence of $Li^+$, $Mg^{2+}$, $Mn^{2+}$, $Ca^{2+}$, $Cs^+$ and $Zn^{2+}$, the fluorescence lifetime of Cy3-O328 did not change or slightly decreased, indicating that these cations did not stabilize or slightly destabilized the secondary structure of

DNA as was suggested earlier for G-quadruplexes [14, 23, 43, 44]. On the other hand, the fluorescence lifetime increased in the presence of $Na^+$, $NH_4^+$, $K^+$ and $Sr^{2+}$, suggesting that these cations stabilized the formation of the secondary structure of DNA. It is worth mentioning that in the context of Cy3-O328 sensor, $Sr^{2+}$ pushes Cy3's lifetime close to the theoretical lifetime of Cy3B (3.19 ns) in the absence of any non-radiative loss [45].

Given that $Na^+$ and $NH_4^+$ are commonly encountered cations, we also investigated the sensitivity of Cy3-O328 to these cations. Similar to the $K^+$-response curve, we measured and plotted the fluorescence lifetimes of the Cy3-O328 sensor in increasing concentrations of these cations (Fig. 3F). The response curves for both cations exhibit similar sigmoidal behaviors to that of $K^+$ and they were also fitted similarly with Eq. (5) (Supplementary Methods). Based on the generated $K_D$ values of these cations, we found that the Cy3-O328 sensor is 100-fold less sensitive to $NH_4^+$ ($K_D$ = 0.6 mM) and 1000-fold less sensitive to $Na^+$ ($K_D$ = 6.8 mM) than it is to $K^+$.

Finally, we tested the possibility of extending our transducing technology to other environmentally sensitive fluorophores. In particular, we replaced Cy3 with Cy5 at the same position in O328 DNA aptamer. The fluorescence lifetime of Cy5-O328 increased in response to an increase in $K^+$ concentration with a sigmoidal signature (Fig. 3D). This response curve overall resembles that of Cy3-O328 with some minor exceptions that are most likely stemming from the structural differences between Cy3 and Cy5. Nevertheless, the results with Cy5-O328 highlight the generality of our transducing technology to other environmentally sensitive fluorophores.

### 3.4 Cy3-O328 potassium sensing ability exhibits very high stability to environmental factors

In complex samples, $Na^+$ and $NH_4^+$ can coexist with $K^+$ and complicate the interpretation of the experimental data, if accurate $K^+$ concentration is of interest. It is widely accepted that the fold difference in the $K_D$ for different ligands gives the relative selectivity of their binding to a common receptor. Nevertheless, this statement is only qualitatively accurate and would be mathematically true only if the binding isotherms would be infinitely steep. In practice the shape of these curves is dictated by the finite and often not very high Hill coefficient. This limited Hill factor produces sigmoidal response curves with elongated tails. In complex mixtures of ligands, these tails can have considerable overlap, which makes quantification more difficult. If the concentration of the species with the highest affinity is of interest, the presence of the other interfering ligand species will result in an apparent increase in the concentration of the species of interest. With the $K^+$ concentration fixed at the value of the $K^+$ dissociation constant, we evaluated the apparent increase in this concentration as a function of the fold excess of $Na^+$ and $NH_4^+$. The analytical function is described by Eq. (25) (Supplementary Methods) and the result is plotted in Fig. 4A. Around the $K^+$ dissociation constant of ~6 μM, Cy3-O328 offers ~15% uncertainty in the measured $K^+$ concentration due to the finite resolution of the time-resolved measurements (Fig. 3B). This uncertainty can be employed to mask the apparent increase in $K^+$ concentration due to the presence of the interfering cations. This 15% contour level is illustrated in Fig. 4A. The area delimited by this 15% contour level and the coordinate axis corresponds to the concentrations of $Na^+$ and $NH_4^+$ that can be successfully masked by the uncertainty of the experimental method. Cy3-O328 allows ~150 concentration fold excess over $K^+$ for $Na^+$ interference alone, and ~9.5 concentration fold excess over $K^+$ for $NH_4^+$ interference alone.

Several data points in the delimited area were experimentally tested and, in all cases, the apparent $K^+$ increase was less than 15% (Fig. 4B), showing that the experimental uncertainty can mask successfully the effect of the interfering cations up to the indicated fold excesses.

Apart from interfering cations, several other factors can influence the Cy3 photophysics or the structure formation in O328. These factors include ionic strength, temperature and pH. We have previously studied the viscosity dependence of Cy3-O328 in order to decouple its deexcitation rates and we showed that the $K^+$ sensing ability is maintained over a wide range of buffer viscosity [16]. In the current study, we also performed the environmental sensitivity experiments on a Cy3-labeled $d(A)_{18}$ oligonucleotide that is not forming secondary structures. This oligonucleotide, named Cy3-Poly(A), serves as a control to determine the effect of the studied environmental factors on the fluorescence of Cy3 inside ssDNA directly, rather than on the $K^+$-induced structure of O328.

Ionic strength had only a minor effect on Cy3-Poly(A) fluorescence. Upon addition of both monovalent CsCl or divalent $ZnCl_2$, the fluorescence of Cy3-Poly(A) decreased only slightly up to concentration as high as 1 M (Figs. S2A and S2B). Therefore, we tested this range with Cy3-O328 in the presence of three $K^+$ concentrations. Cy3-O328 maintained its $K^+$-sensing ability over the whole monovalent $Cs^+$ titration up to 1 M (Fig. 4C). In the case of divalent $Zn^{2+}$ the sensing ability is largely maintained up to ~1 mM $ZnCl_2$. These values indicate that the $K^+$-sensing ability of Cy3-O328 is maintained up to ionic strengths generated by monovalent and divalent cations concentration that are hundreds of folds above the $K^+$ dissociation constant.

Cyanine dyes owe their fluorescence properties mainly to their ability to undergo cis-trans photoisomerization in the excited state. Photoisomerization has to cross an energy barrier and therefore its rate is dictated by an Arrhenius-type equation (Supplementary Methods). This renders cyanine dyes photoisomerization and therefore fluorescence to be temperature-dependent. In case of Cy3-Poly(A), that lacks any secondary structure, the temperature dependence described by Eq. (20) fit very well the experimental data (Fig. S2C). As described in the Methods Section, for simplicity, the experimental temperature-dependence of Cy3-O328 was fit to a piecewise linear model (Fig. 4E). The $K^+$-sensing ability of Cy3-O328 is largely maintained between 5 °C and 45 °C. Nevertheless, according to the van't Hoff equation, an increase in the $K^+$ dissociation constant is observed with increasing the temperature. Therefore, for practical applications the calibration curve described in Fig. 2D at 25 °C, should be recalculated at different temperatures and the temperature-dependence of the $K_D$ should be considered if the experiments are performed at a temperature other than 25 °C.

Cy3-Poly(A) presented excellent stability to pH variations in the range of pH 6.5 to pH 9.0. Similarly, Cy3-O328 maintained its $K^+$-sensing ability over this whole pH range. Taken together, the environmental stability of Cy3-O328 $K^+$-sensing ability suggests that Cy3-O328 can be used in a variety of environments for $K^+$ concentration measurements with minimum error.

Equipped with this extensive characterization of Cy3-O328 as a $K^+$ sensor, we employed it to determine the $K^+$ equivalent concentration of several test samples. All the samples were serially diluted in 1:10 series until the fluorescence lifetime of Cy3-O328 in the respective test solution was brought down towards 2.3 ns, which corresponds to the $K^+$ dissociation constant. Once the

lifetime was decreased to a value within the $EC_{10}$-$EC_{90}$ interval, the equivalent $K^+$ concentration was determined by using Eq. (11) (Supplementary Methods) and considering the final dilution factor. For all test samples, the resulting $K^+$ equivalent concentration is in very good agreement with the reference values (Table 1). At the end of each measurement, saturating KCl concentration was added to each sample. Cy3-O328 responded by an increase in its fluorescence lifetime close to its upper limit value (Table S1). This KCl addition experiment shows that, for all the measured test samples, the $K^+$-sensitivity of Cy3-O328 is not altered by any environmental factor and that the increased fluorescent signal is $K^+$-specific even in more complex environments.

## 4. Discussion

The ease of use and adaptability of DNA aptamers and DNAzymes, especially G-quadruplexes, provide working platforms for versatile detection of ions, organic molecules, nucleic acids, and proteins [10-13, 24-26, 29, 33, 46-49]. In addition to their diverse sensitivities, these DNA aptamers could potentially be coupled with a wide range of signal transducing mechanisms, including fluorescence through FRET, or "turn-on"/ "turn-off" mechanisms through other luminescent, fluorescent or colorimetric add-in factors, such as crystal violet or berberine [1, 3, 28, 50]. In principle, the sensing mechanism in DNA aptamers depends on the ligand inducing a DNA conformational change that is followed by transducing a measurable signal by an indirect external reporter. Here, we introduced a fluorescent transducing technology with a single fluorophore (Cy3) embedded in a DNA aptamer. Our transducing technology bypasses the requirement of an indirect external reporter and the dual labeling in case of FRET. It also extends the use of fluorescence enhancement in the context of PIFE to other protein-free systems.

The environmental sensitivity of Cy3 to structural changes in DNA coupled with the sensitivity of O328 to $K^+$ ions gave rise to an effective potassium sensor with a working range of 0.44 to 250 μM. Cy3-O328 directly transduces the signal as an increase in Cy3 fluorescence. Our technology offers the advantage of coupling the biorecognition and transducing elements in one single DNA-Dye molecule that is easily customizable and available through different venders at efficient costs. The excellent agreement between Cy3-O328 steady-state fluorescence and time-resolved fluorescence lifetimes signal readout allows for an almost interchangeable applicability of both measurements up to the availability of the machinery and user preference.

The quality of a biosensor is based on five characteristics: stability, reproducibility, linearity, sensitivity, and selectivity [41]. As a DNA aptamer, our sensor is stable, and with time-resolved fluorescence lifetime measurements, it also achieves great reproducibility. Moreover, our sensor exhibits an almost linear response between 0.44 and 250 μM of $K^+$ over a dynamic fluorescence lifetime range of 1 ns. The most important characteristics of a biosensor are sensitivity and selectivity. Our sensor's sensitivity is comparable to, if not better than, established $K^+$-sensors [7, 28, 30-32, 51-53]. In the context of physiological samples, the most relevant interfering ions for potassium sensors are sodium ions. Our sensor provides over a 1000-fold higher sensitivity to $K^+$ ($K_D$=6 μM) than to $Na^+$ ($K_D$=6.8 mM) (Fig. 3F) even though most biological samples maintain less than a 100-fold excess of $Na^+$ over $K^+$ [28, 30, 54]. Up to 150-fold higher $Na^+$ than $K^+$, Cy3-O328 can be considered to measure exclusively the potassium with an error lower than the experimental uncertainty (Figs. 3B, 4A and 4B). We therefore propose that our sensor can be

used on physiological samples. Different monovalent and divalent ions other than $K^+$ have been shown to coordinate G-quadruplexes, including $NH_4^+$, $Na^+$ and $Sr^{2+}$ [27, 55, 56]. These ions seem to coordinate our DNA aptamer, which potentially might make it a versatile sensor with further modulation in its binding selectivity. Moreover, O328 $K^+$-sensing ability is maintained with very good stability over a wide range of environmental factors such as ionic strength, temperature, pH and interfering cations (Fig. 4). When employed in determining the equivalent $K^+$ concentrations of test samples, O328 excelled through its ease of use and a simple sample preparation protocol, while still giving relatively accurate results (Table T1).

In conclusion, we believe that our transducing technology can be adopted in the development of various small molecule biosensors. For example, modulating the sequence can tailor our sensor from a specific ligand to another. Our DNA aptamer can also be integrated into other DNA sequences for different functionalities. In addition, more generally, Cy3-conjugated DNA aptamers, other than O328, can be employed not only to detect small molecules but also to measure other important environmental changes, such as temperature and viscosity. In case of different DNA structures without ligand binding, Cy3 has already been successfully used as a single label to monitor a series of DNA effects such as opposite strand hybridization [16], sequence dependence of fluorescence of cyanine-labeled DNA [38] and DNA hairpin dynamics [57]. However, the aptamer design should take into consideration the conjugation position of Cy3 such that it does not alter the sensor's recognition and sensitivity to structural rearrangement. Furthermore, other environmentally sensitive fluorophores can be considered when green dyes are not favorable. We illustrated this extrapolation in the current study by using Cy5-O328 and showed that it maintained the capabilities of a sensor.

One of the main limitations yet to be overcome, in the case of ssDNA aptamers, is that the presence of ssDNA-binding proteins can melt the specific secondary structures and remove the ligand-induced fluorescent modulation [16]. A similar limitation is also imposed by the presence of ssDNA-specific nucleases that would biochemically deteriorate the aptamer. In order to measure the concentration of various ligands of interest in complex environments where such proteins are present, one would have to first denature the proteins and then perform the measurements.

As a future direction, the single dye-conjugation aptamer in our design makes it easier to use multiple aptamers, each with separable fluorescence spectra and different metal ion sensitivities, to monitor the concentrations of different small molecules simultaneously in an unknown sample. Finally, we anticipate that cyanine dyes in general can be engineered to host side functional groups that could play a role in stabilizing or destabilizing the overall structure of the aptamer.

Funding: This work was supported by King Abdullah University of Science and Technology under Grant CRG6 (URF/1/3432- 01- 01) to S.M.H.

Notes

The authors declare no competing financial interest.

**Acknowledgements**

The authors are grateful to Prof. Stefan T. Arold (KAUST) for providing access to the time-resolved fluorescence spectrophotometer. We thank Prof. Satoshi Habuchi for helpful discussions. We thank Daniela-Violeta Raducanu for her support in some experiments. The authors would like to acknowledge Iwona Czaban for her support in the CD experiment. We are grateful to members of Samir M. Hamdan's lab for helpful discussions.

## References

[1] B. Ruttkay-Nedecky, J. Kudr, L. Nejdl, D. Maskova, R. Kizek, V. Adam, G-quadruplexes as sensing probes, Molecules (Basel, Switzerland), 18(2013) 14760-79.
[2] Y. Xiang, Y. Lu, DNA as sensors and imaging agents for metal ions, Inorganic chemistry, 53(2014) 1925-42.
[3] X.B. Zhang, R.M. Kong, Y. Lu, Metal ion sensors based on DNAzymes and related DNA molecules, Annual review of analytical chemistry (Palo Alto, Calif), 4(2011) 105-28.
[4] S. Vigneshvar, C.C. Sudhakumari, B. Senthilkumaran, H. Prakash, Recent Advances in Biosensor Technology for Potential Applications - An Overview, Frontiers in bioengineering and biotechnology, 4(2016) 11.
[5] Y. Du, S. Dong, Nucleic Acid Biosensors: Recent Advances and Perspectives, Anal Chem, 89(2017) 189-215.
[6] Y. Lu, J. Liu, Functional DNA nanotechnology: emerging applications of DNAzymes and aptamers, Current opinion in biotechnology, 17(2006) 580-8.
[7] S. Nagatoishi, T. Nojima, E. Galezowska, B. Juskowiak, S. Takenaka, G quadruplex-based FRET probes with the thrombin-binding aptamer (TBA) sequence designed for the efficient fluorometric detection of the potassium ion, Chembiochem : a European journal of chemical biology, 7(2006) 1730-7.
[8] H. Ueyama, M. Takagi, S. Takenaka, A novel potassium sensing in aqueous media with a synthetic oligonucleotide derivative. Fluorescence resonance energy transfer associated with Guanine quartet-potassium ion complex formation, Journal of the American Chemical Society, 124(2002) 14286-7.
[9] F. He, Y. Tang, S. Wang, Y. Li, D. Zhu, Fluorescent amplifying recognition for DNA G-quadruplex folding with a cationic conjugated polymer: a platform for homogeneous potassium detection, Journal of the American Chemical Society, 127(2005) 12343-6.
[10] T. Li, S. Dong, E. Wang, Label-free colorimetric detection of aqueous mercury ion (Hg2+) using Hg2+-modulated G-quadruplex-based DNAzymes, Anal Chem, 81(2009) 2144-9.
[11] L. Guo, D. Nie, C. Qiu, Q. Zheng, H. Wu, P. Ye, et al., A G-quadruplex based label-free fluorescent biosensor for lead ion, Biosensors & bioelectronics, 35(2012) 123-7.
[12] K.H. Leung, H.Z. He, H.J. Zhong, L. Lu, D.S. Chan, D.L. Ma, et al., A highly sensitive G-quadruplex-based luminescent switch-on probe for the detection of polymerase 3'-5' proofreading activity, Methods (San Diego, Calif), 64(2013) 224-8.
[13] K. Qu, C. Zhao, J. Ren, X. Qu, Human telomeric G-quadruplex formation and highly selective fluorescence detection of toxic strontium ions, Molecular bioSystems, 8(2012) 779-82.
[14] D. Bhattacharyya, G. Mirihana Arachchilage, S. Basu, Metal Cations in G-Quadruplex Folding and Stability, Frontiers in chemistry, 4(2016) 38.

[15] S. Umrao, V. Jain, Anusha, B. Chakraborty, R. Roy, Protein-induced fluorescence enhancement as aptamer sensing mechanism for thrombin detection, Sensor Actuat B-Chem, 267(2018) 294-301.
[16] F. Rashid, V.S. Raducanu, M.S. Zaher, M. Tehseen, S. Habuchi, S.M. Hamdan, Initial state of DNA-Dye complex sets the stage for protein induced fluorescence modulation, Nat Commun, 10(2019) 2104.
[17] M. Levitus, S. Ranjit, Cyanine dyes in biophysical research: the photophysics of polymethine fluorescent dyes in biomolecular environments, Quarterly reviews of biophysics, 44(2011) 123-51.
[18] M.E. Sanborn, B.K. Connolly, K. Gurunathan, M. Levitus, Fluorescence properties and photophysics of the sulfoindocyanine Cy3 linked covalently to DNA, J Phys Chem B, 111(2007) 11064-74.
[19] A. Bottcher, D. Kowerko, R.K. Sigel, Explicit analytic equations for multimolecular thermal melting curves, Biophys Chem, 202(2015) 32-9.
[20] D.J.G. Ives, Chemical thermodynamics: with special reference to inorganic chemistry, London,: Macdonald and Co.; 1971.
[21] P.W. Atkins, J. De Paula, Atkins' Physical chemistry, 8th ed., Oxford ; New York: Oxford University Press; 2006.
[22] J. D'Errico, SLM-shape language modeling, Matlab Central, (2009).
[23] S.W. Blume, V. Guarcello, W. Zacharias, D.M. Miller, Divalent transition metal cations counteract potassium-induced quadruplex assembly of oligo(dG) sequences, Nucleic Acids Res, 25(1997) 617-25.
[24] H. Bo, C. Wang, Q. Gao, H. Qi, C. Zhang, Selective, colorimetric assay of glucose in urine using G-quadruplex-based DNAzymes and 10-acetyl-3,7-dihydroxy phenoxazine, Talanta, 108(2013) 131-5.
[25] Y. Du, B. Li, S. Guo, Z. Zhou, M. Zhou, E. Wang, et al., G-Quadruplex-based DNAzyme for colorimetric detection of cocaine: using magnetic nanoparticles as the separation and amplification element, The Analyst, 136(2011) 493-7.
[26] D. Hu, F. Pu, Z. Huang, J. Ren, X. Qu, A quadruplex-based, label-free, and real-time fluorescence assay for RNase H activity and inhibition, Chemistry (Weinheim an der Bergstrasse, Germany), 16(2010) 2605-10.
[27] B.I. Kankia, L.A. Marky, Folding of the thrombin aptamer into a G-quadruplex with Sr(2+): stability, heat, and hydration, Journal of the American Chemical Society, 123(2001) 10799-804.
[28] D.M. Kong, J.H. Guo, W. Yang, Y.E. Ma, H.X. Shen, Crystal violet-G-quadruplex complexes as fluorescent sensors for homogeneous detection of potassium ion, Biosensors & bioelectronics, 25(2009) 88-93.
[29] R. Li, C. Xiong, Z. Xiao, L. Ling, Colorimetric detection of cholesterol with G-quadruplex-based DNAzymes and ABTS2, Analytica chimica acta, 724(2012) 80-5.
[30] S. Nagatoishi, T. Nojima, B. Juskowiak, S. Takenaka, A pyrene-labeled G-quadruplex oligonucleotide as a fluorescent probe for potassium ion detection in biological applications, Angewandte Chemie (International ed in English), 44(2005) 5067-70.
[31] H. Qin, J. Ren, J. Wang, N.W. Luedtke, E. Wang, G-quadruplex-modulated fluorescence detection of potassium in the presence of a 3500-fold excess of sodium ions, Anal Chem, 82(2010) 8356-60.
[32] X. Yang, T. Li, B. Li, E. Wang, Potassium-sensitive G-quadruplex DNA for sensitive visible potassium detection, The Analyst, 135(2010) 71-5.

[33] X.H. Zhou, D.M. Kong, H.X. Shen, G-quadruplex-hemin DNAzyme-amplified colorimetric detection of Ag+ ion, Analytica chimica acta, 678(2010) 124-7.
[34] T. Wu, C.J. Zhang, Z.P. Wang, H.X. Ren, Y. Kang, Y.P. Du, Tuning the sensing range of potassium ions by changing the loop size of G-quadruplex sensors, New J Chem, 40(2016) 9285-90.
[35] A. Marchand, V. Gabelica, Folding and misfolding pathways of G-quadruplex DNA, Nucleic Acids Res, 44(2016) 10999-1012.
[36] C. Liu, B. Zhou, Y. Geng, D. Yan Tam, R. Feng, H. Miao, et al., A chair-type G-quadruplex structure formed by a human telomeric variant DNA in K(+) solution, Chem Sci, 10(2019) 218-26.
[37] K. Palo, L. Brand, C. Eggeling, S. Jager, P. Kask, K. Gall, Fluorescence intensity and lifetime distribution analysis: toward higher accuracy in fluorescence fluctuation spectroscopy, Biophysical journal, 83(2002) 605-18.
[38] N. Kretschy, M. Sack, M.M. Somoza, Sequence-Dependent Fluorescence of Cy3- and Cy5-Labeled Double-Stranded DNA, Bioconjug Chem, 27(2016) 840-8.
[39] C. Agbavwe, M.M. Somoza, Sequence-dependent fluorescence of cyanine dyes on microarrays, PloS one, 6(2011) e22177.
[40] E. Altszyler, A.C. Ventura, A. Colman-Lerner, A. Chernomoretz, Ultrasensitivity in signaling cascades revisited: Linking local and global ultrasensitivity estimations, PloS one, 12(2017) e0180083.
[41] N. Bhalla, P. Jolly, N. Formisano, P. Estrela, Introduction to biosensors, Essays in biochemistry, 60(2016) 1-8.
[42] B.N. Kholodenko, J.B. Hoek, H.V. Westerhoff, G.C. Brown, Quantification of information transfer via cellular signal transduction pathways, FEBS letters, 414(1997) 430-4.
[43] C.C. Hardin, A.G. Perry, K. White, Thermodynamic and kinetic characterization of the dissociation and assembly of quadruplex nucleic acids, Biopolymers, 56(2000) 147-94.
[44] S. Neidle, S. Balasubramanian, Quadruplex Nucleic Acids, Cambridge: RSC: Biomoleculer Sciences; 2006.
[45] M. Cooper, A. Ebner, M. Briggs, M. Burrows, N. Gardner, R. Richardson, et al., Cy3B: improving the performance of cyanine dyes, Journal of fluorescence, 14(2004) 145-50.
[46] T. Li, G. Liang, X. Li, Chemiluminescence assay for the sensitive detection of iodide based on extracting Hg2+ from a T-Hg(2+)-T complex, The Analyst, 138(2013) 1898-902.
[47] H. Li, Z. Wu, L. Qiu, J. Liu, C. Wang, G. Shen, et al., Ultrasensitive label-free amplified colorimetric detection of p53 based on G-quadruplex MBzymes, Biosensors & bioelectronics, 50(2013) 180-5.
[48] X.P. Wang, B.C. Yin, P. Wang, B.C. Ye, Highly sensitive detection of microRNAs based on isothermal exponential amplification-assisted generation of catalytic G-quadruplex DNAzyme, Biosensors & bioelectronics, 42(2013) 131-5.
[49] B. Jiang, M. Wang, C. Li, J. Xie, Label-free and amplified aptasensor for thrombin detection based on background reduction and direct electron transfer of hemin, Biosensors & bioelectronics, 43(2013) 289-92.
[50] Y. Liu, B. Li, D. Cheng, X. Duan, Simple and sensitive fluorescence sensor for detection of potassium ion in the presence of high concentration of sodium ion using berberine–G-quadruplex complex as sensing element, Microchemical Journal, 99(2011) 503-7.
[51] C. Shi, H. Gu, C. Ma, An aptamer-based fluorescent biosensor for potassium ion detection using a pyrene-labeled molecular beacon, Anal Biochem, 400(2010) 99-102.

[52] A.E. Radi, C.K. O'Sullivan, Aptamer conformational switch as sensitive electrochemical biosensor for potassium ion recognition, Chemical communications (Cambridge, England), (2006) 3432-4.
[53] L. Wang, X. Liu, X. Hu, S. Song, C. Fan, Unmodified gold nanoparticles as a colorimetric probe for potassium DNA aptamers, Chemical communications (Cambridge, England), (2006) 3780-2.
[54] S.A. George, K.J. Sciuto, J. Lin, M.E. Salama, J.P. Keener, R.G. Gourdie, et al., Extracellular sodium and potassium levels modulate cardiac conduction in mice heterozygous null for the Connexin43 gene, Pflugers Archiv : European journal of physiology, 467(2015) 2287-97.
[55] N.V. Hud, P. Schultze, V. Sklenar, J. Feigon, Binding sites and dynamics of ammonium ions in a telomere repeat DNA quadruplex, Journal of molecular biology, 285(1999) 233-43.
[56] G. Laughlan, A.I. Murchie, D.G. Norman, M.H. Moore, P.C. Moody, D.M. Lilley, et al., The high-resolution crystal structure of a parallel-stranded guanine tetraplex, Science (New York, NY), 265(1994) 520-4.
[57] M.J. Morten, S.G. Lopez, I.E. Steinmark, A. Rafferty, S.W. Magennis, Stacking-induced fluorescence increase reveals allosteric interactions through DNA, Nucleic Acids Res, 46(2018) 11618-26.
[58] R.P. Traslavina, E.J. King, A.S. Loar, E.R. Riedel, M.S. Garvey, R. Ricart-Arbona, et al., Euthanasia by CO(2) inhalation affects potassium levels in mice, J Am Assoc Lab Anim Sci, 49(2010) 316-22.
[59] B.M. Christensen, R. Perrier, Q. Wang, A.M. Zuber, M. Maillard, D. Mordasini, et al., Sodium and potassium balance depends on alphaENaC expression in connecting tubule, J Am Soc Nephrol, 21(2010) 1942-51.

## Narrative Biographies

Mr Vlad-Stefan Raducanu obtained his MSc from King Abdullah University and is currently pursuing his PhD studies at the same university. Mr Raducanu is a physicist by training and his research interest has been focusing on developing a variety of bioimaging and biosensors approaches. His research combines biochemical and single molecule bioimaging approaches to study the mechanisms involved in DNA replication and repair at the single molecule level.

Dr Fahad Rashid obtained his PhD from King Abdullah University of Science and Technology and is currently doing his postdoctoral training at Johns Hopkins Medical School. His research interest is focused on using single molecule imaging and structural techniques to study the mechanisms involved in DNA replication and repair.

Dr Manal Zaher obtained her PhD from King Abdullah University of Science and Technology and is currently doing her postdoctoral training at Harvard Medical School. Her research interest is focused on using single molecule imaging and structural techniques to study the mechanisms involved in DNA replication and repair.

Dr Yanyan Li obtained her PhD from China Pharmaceutical University and is currently doing her postdoctoral training at King Abdullah University of Science and Technology. Her research interest is focused on studying the mechanisms involved in cell migration and homing to specific sites within the body.

Prof Jasmeen Merzaban obtained her PhD from University of British Columbia and did her postdoctoral Training at Harvard Medical School. Prof Merzaban is Associate Professor of Biosciences and Principal Investigator of the Laboratory of Cell Migration and Signaling at King Abdullah University of Science and Technology. Prof Merzaban's research interests focus on understanding and optimizing the mechanism by which immune and stem cells exit the blood circulation to "home" to specific sites within the body. This process is mediated by sophisticated and coordinated steps controlled by multiple signaling and adhesion molecules, with key players being the selectins.

Prof Samir M. Hamdan obtained his PhD from Australian National University and did his postdoctoral training at Harvard Medical School. Prof Hamdan is Associate Dean of Division of Biological and Environmental Sciences and Engineering, Associate Professor of Biosciences and Principal Investigator of the Laboratory of DNA Replication and Recombination at King Abdullah University of Science and Technology. Professor Hamdan's research interest is focused on the reconstitution, imaging and characterization of multi-protein nucleic acid binding machineries at the single molecule level. Toward achieving this goal his lab uses an approach that combines conventional biochemical and biophysical tools with wide range of force and fluorescence single-molecule imaging techniques.

## Figure Legends

**Fig. 1.** Cy3 transduces conformational changes induced by metal ions in DNA aptamers through a modulation of its fluorescence properties. (A) Schematic illustrating the proposed transducing technology. (B) A plot of time-resolved fluorescence lifetimes of Cy3-labeled G1 versus the dimensionless $\log_{10}$ of $K^+$ concentration normalized to 1 nM. The curve was fit to Eq. (5) (Supplementary Methods) with a fixed starting point at $\tau_0 = 1.9$ ns. The dissociation constant ($K_D$) and the apparent Hill coefficient (n*) are reported. $\tau_\infty$ denotes the maximum fluorescence lifetime achieved.

**Fig. 2.** Building a potassium sensor with embedded Cy3 transducer. (A) CD spectra of 20 μM of unlabeled O328 with increasing concentrations of $K^+$. The inset shows the total absorbance spectra of unlabeled O328 for the measured $K^+$ concentrations. (B) Bar chart showing the fluorescence lifetimes of O328 labeled with Cy3 at various positions through phosphoramidite linkage, measured in water (light blue) or 50 mM KCl (dark blue). The sequence of O328 and the positions at which Cy3 is inserted are displayed above the bar chart. (C) Time-resolved fluorescence decays of Cy3-O328 with increasing concentrations of $K^+$ (0 – 1 M). (D) A plot of the time-resolved fluorescence lifetimes versus the dimensionless $\log_{10}$ of $K^+$ concentration normalized to 1 nM. The curve was fit to Eq. (5) (Supplementary Methods) with a fixed starting point at $\tau_0 = 1.8$ ns. The dissociation constant ($K_D$) and the apparent Hill coefficient (n*) are reported. $\tau_\infty$ denotes the maximum fluorescence lifetime achieved. Vertical dashed lines indicate the limits of $EC_{10}$ and $EC_{90}$ as described in Supplementary Methods. (E) Emission spectra (520 – 700 nm) of Cy3-O328 upon excitation at 535 nm with increasing concentrations of $K^+$ (0 – 1 M). Spectra are color coded as shown in the included inset table. (F) Plots of normalized fluorescence percentage change of Cy3-O328, described by Eq. (1) (Supplementary Methods), as a function of $\log_{10}$ of the $K^+$ concentration normalized to 1 nM. The results are derived from time-resolved and steady-state measurements. The Pearson coefficient of the correlation between the two measurements is reported in the interval between $EC_{10}$ and $EC_{90}$.

**Fig. 3.** Characterization of Cy3-O328 as a potassium sensor. (A) A plot of the local response coefficient as a percentage, described by Eq. (9) (Supplementary Methods), versus the dimensionless $\log_{10}$ of $K^+$ concentration normalized to 1 nM. The $C_R$ value at which the maximum response is achieved is indicated by the red vertical line residing inside the interval between $EC_{10}$ and $EC_{90}$, in the vicinity of the $K_D$. A response between 2% and 9% is generated in the interval between $EC_{10}$ and $EC_{90}$, when transducing from the $K^+$ concentration to the fluorescence lifetime (ns). (B) A plot of the theoretical relative uncertainty in the measured $K^+$ concentration versus the dimensionless $\log_{10}$ of the $K^+$ concentration normalized to 1 nM in the interval between $EC_{10}$ and $EC_{90}$ using our sensor. The plot is generated as a parametric curve with the y-coordinate given by Eq. (15) (Supplementary Methods) and the x-coordinate given by Eq. (8) (Supplementary Methods) and varying the parameter $\tau$ between 1.9 ns (10% response) and 2.73 ns (90% response). The concentration at which the minimum uncertainty is achieved, $C_E$, is indicated by the red vertical dashed line. The uncertainty of the lifetime measurements is indicated as $\Delta\tau$=25 ps. (C) A plot of the inverse function of the response function described by the curve in Fig. 2D; i.e. a plot of the dimensionless $\log_{10}$ of the $K^+$ concentration normalized to 1 nM versus the fluorescence lifetime as described by Eq. (11) (Supplementary Methods). The shaded area marks the working range of the concentrations that we propose for our sensor. This area is delimited by $EC_{10}$ and $EC_{90}$

on the y-axis and by the fluorescent lifetimes in ns corresponding to these concentrations on the x-axis. (D) A plot of time-resolved fluorescence lifetimes of Cy5-O328 versus the dimensionless $\log_{10}$ of the $K^+$ concentration normalized to 1 nM. The curve was fit to Eq. (5) (Supplementary Methods) with a fixed starting point at $\tau_0 = 1.57$ ns. The dissociation constant ($K_D$) and the apparent Hill coefficient (n*) are reported. Vertical dashed lines represent the limits of $EC_{10}$ and $EC_{90}$ described in Supplementary Methods. (E) A bar chart representing the time-resolved fluorescence lifetimes of Cy3-O328 in the presence of water or 10 mM of various salts. (F) Three lifetime response curves of Cy3-O328 in the presence of increasing concentrations of KCl (blue), $NH_4Cl$ (red) and NaCl (green) as a function of $\log_{10}$ of the corresponding salt concentration normalized to 1 nM. Curves are fitted as described above.

**Fig. 4.** Characterization of the environmental sensitivity of potassium sensing by Cy3-O328. (A) Contour color plot of the apparent increase in $K^+$ concentration determined using Cy3-O328, as a function of the concentration fold excess of $NH_4^+$ over $K^+$ and of the concentration fold excess of $Na^+$ over $K^+$. The datapoints marked by the red crosses were experimentally tested. The contour color plot was generated using Eq. (25) and Eq. (11) (Supplementary Methods). The contour level lines are shown in black in 15% increments. (B) Bar chart showing the experimental apparent increase in $K^+$ concentration determined using Cy3-O328 at different fold excess of $NH_4^+$ and $Na^+$ over $K^+$. The blue dashed line indicates the 15% uncertainty threshold of the time-resolved measurements around the $K^+$ dissociation constant ($K_D$). (C) Bar chart showing the fluorescence lifetime of Cy3-O328 in increasing ionic strength of monovalent cations as titration of CsCl salt concentration. Datapoints were collected in water (blue), 6 μM KCl (red) and 10 mM KCl (green). (D) Bar chart showing the fluorescence lifetime of Cy3-O328 in increasing ionic strength of divalent cations as titration of $ZnCl_2$ salt concentration. Datapoints were collected in water (blue), 6 μM KCl (red) and 10 mM KCl (green). (E) Temperature dependence of fluorescence emission intensity of Cy3-O328 in water (blue), 6 μM KCl (red) and 10 mM KCl (green). The experimental data points were fit to a linear piecewise model by SLM tool (as described in the Methods section). Slopes and endpoints are indicated for each linear segment and for each KCl concentration with the appropriate color. All the indicated slopes have the unites of $10^5$ A.U./°C. The goodness of fit is determined from the indicated global $R^2$ value for each KCl concentration. (D) Bar chart showing the fluorescence lifetime of Cy3-O328 at different pH points of the buffer. The buffering reagent for the whole pH range was 50 mM Trizma Pre-set crystals of the desired pH.

Fig 1

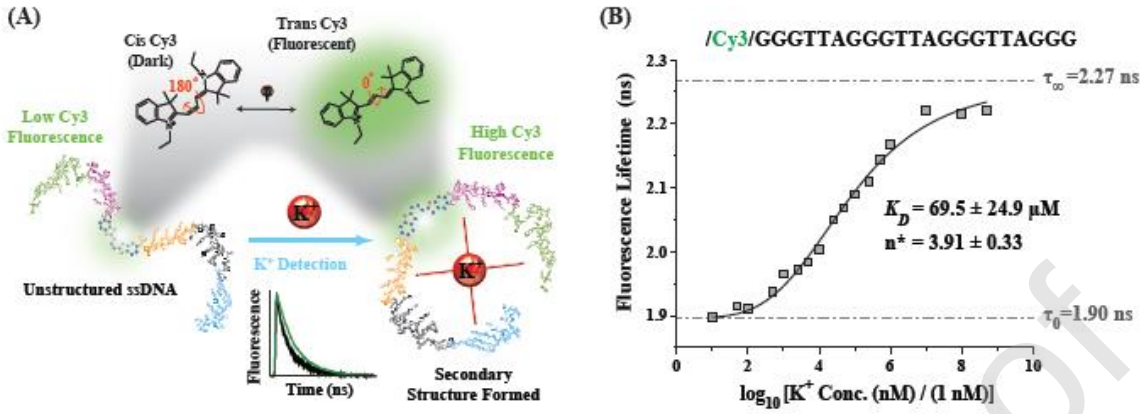

Fig 2

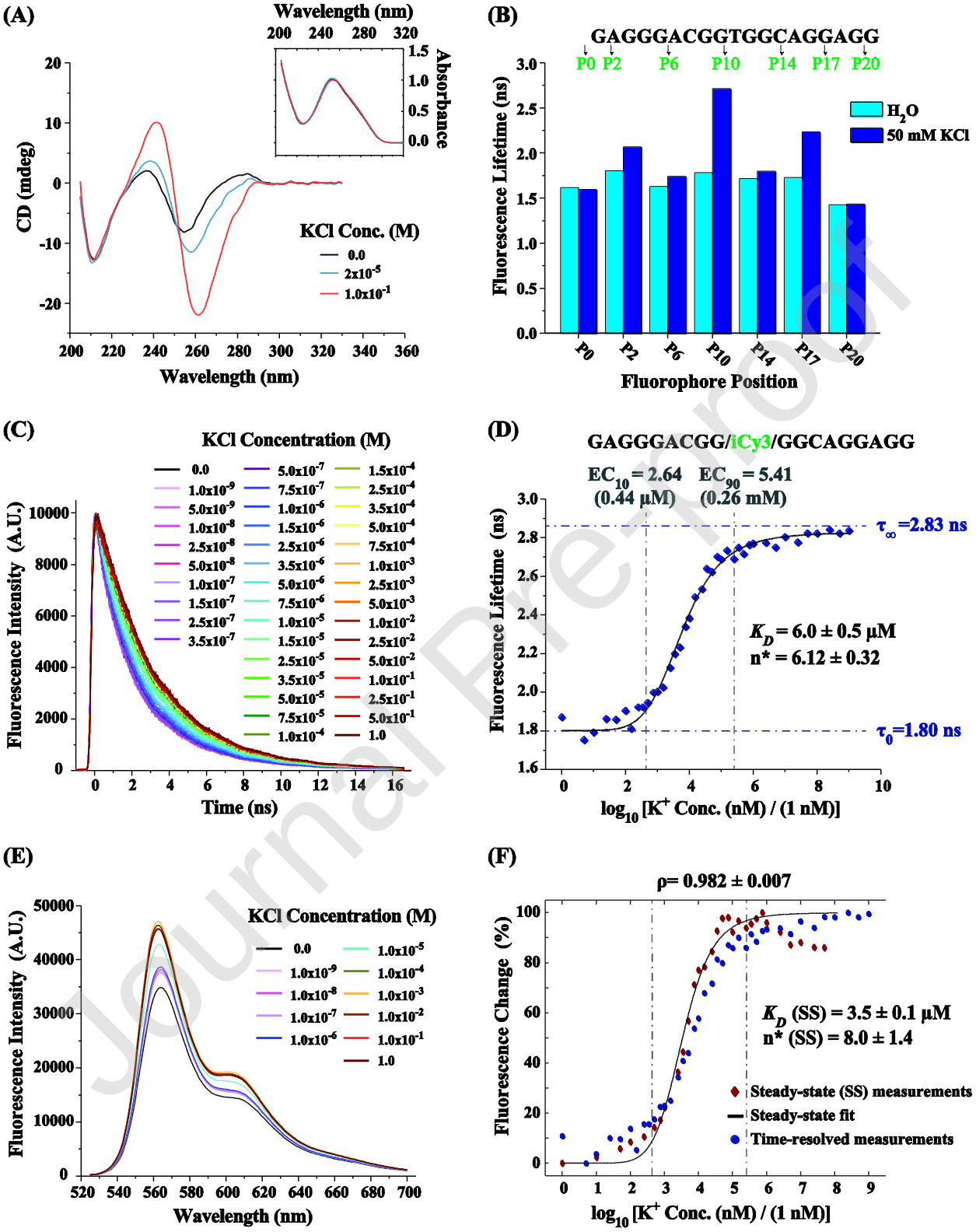

Fig 3

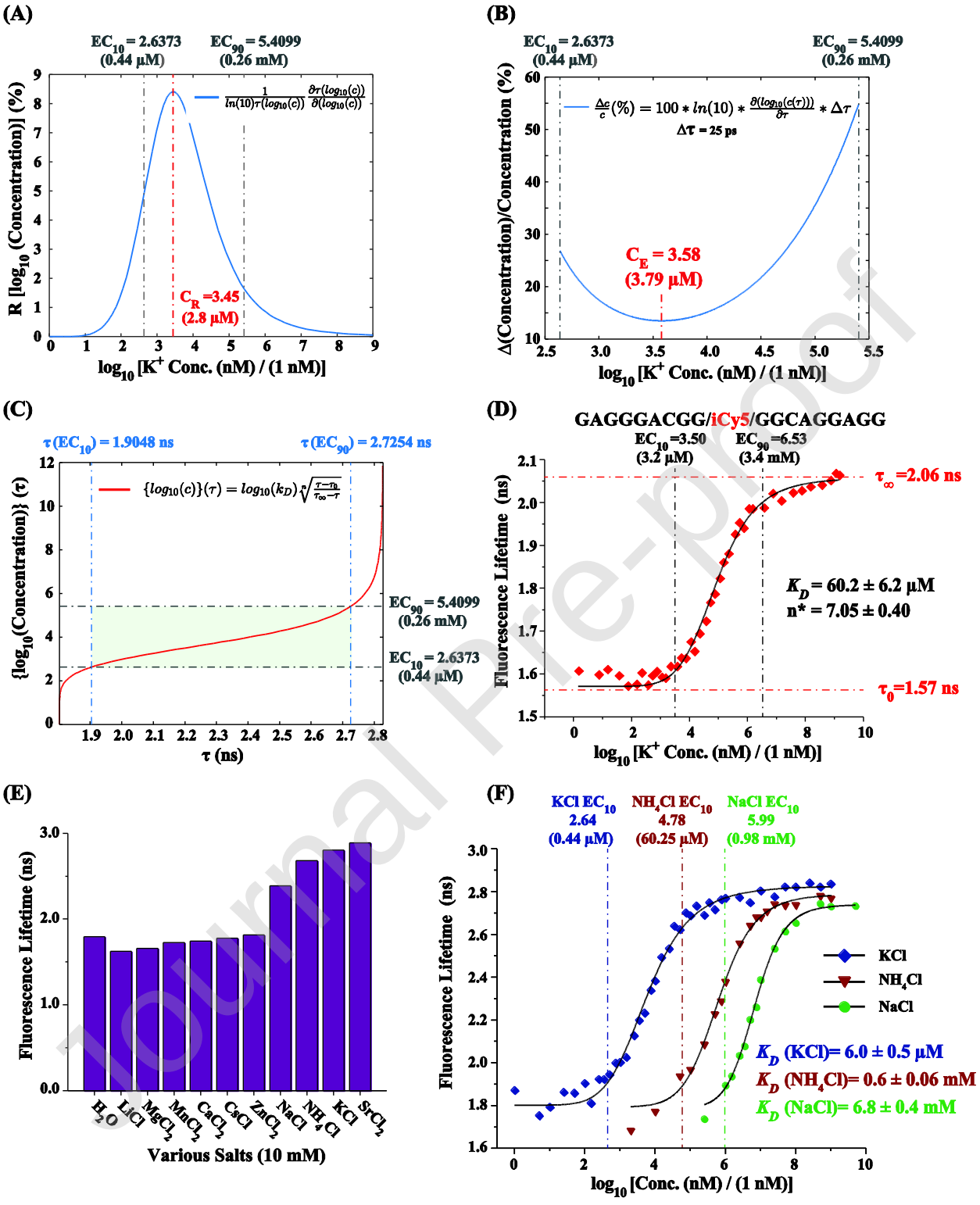

Fig 4

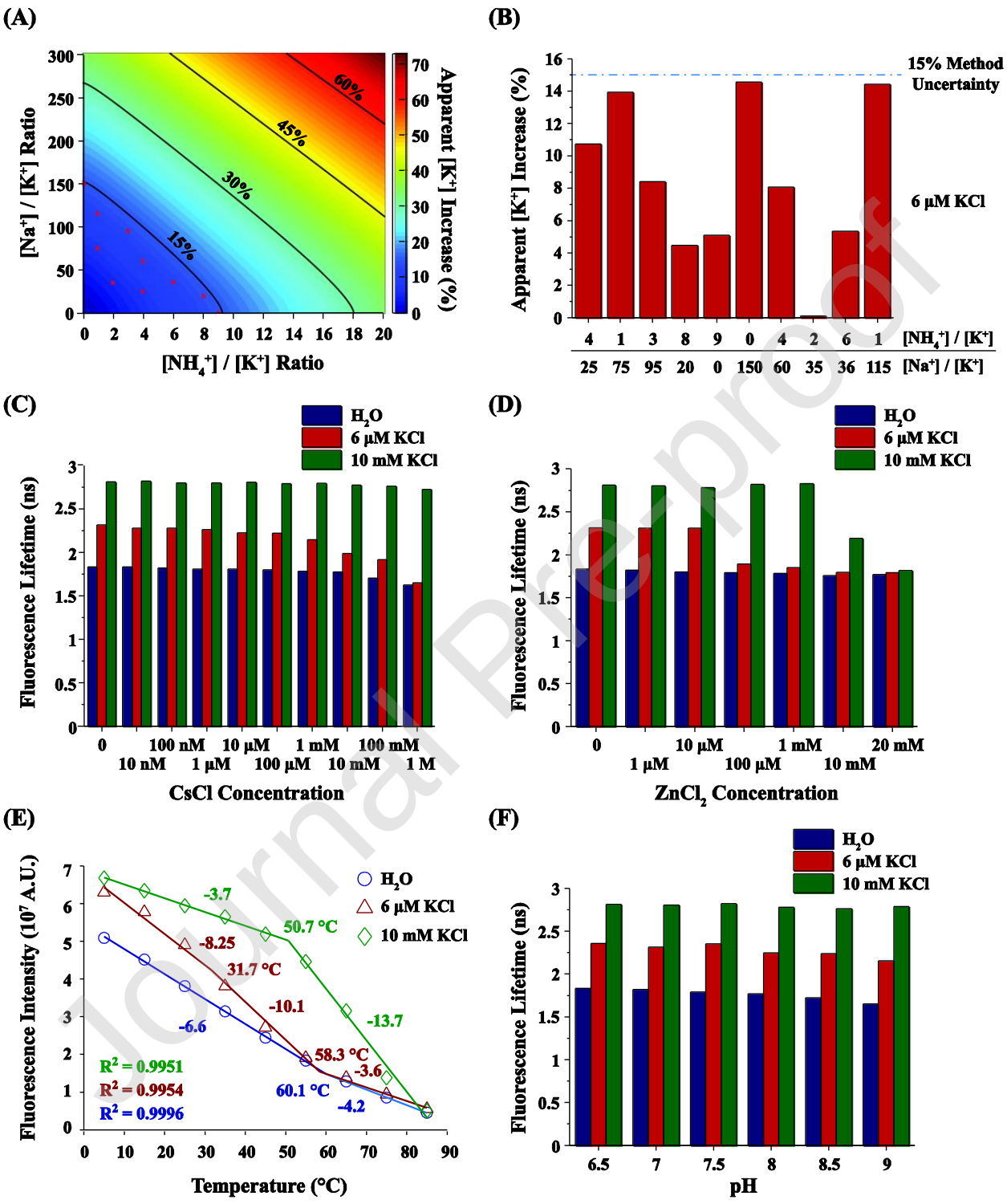

## Table

**Table 1.** Determination of $K^+$ equivalent concentration for a series of test samples using Cy3-O328 fluorescence lifetime measurements and Eq. (11). The parameters used in Eq. (11) are the obtained numerically in Fig. 2D from the fitting of the calibration curve.

| Sample | Reference Potassium | Reference Source | Dilution Factor | | O328-Cy3 Lifetime (ns) | | | Measured $K^+$ Concentration (μM) | | | Measured $K^+$ Concentration |
|---|---|---|---|---|---|---|---|---|---|---|---|
| | | | | | Repeat 1 | Repeat 2 | Repeat 3 | Repeat 1 | Repeat 2 | Repeat 3 | |
| Bottled drinking water 1 | 17.9 μM | Label | 2 | | 2.32 | 2.36 | 2.33 | 12.1 | 15.0 | 13.1 | 13.4 ± 1.5 μM |
| Bottled drinking water 2 | 127.9 μM | Label | 200 | | 1.97 | 1.94 | 1.98 | 152.7 | 124.4 | 166.5 | 147.9 ± 21.5 μM |
| Bottled drinking water 3 | 204.6 μM | Label | 200 | | 2.00 | 2.03 | 2.01 | 202.8 | 240.7 | 214.4 | 219.3 ± 19.4 μM |
| Potassium standard 10 ppm | 255.8 μM | Material data sheet | 20 | | 2.43 | 2.43 | 2.39 | 232.7 | 241.6 | 187.8 | 227.3 ± 22.1 μM |
| | | | 200 | | 2.02 | 2.04 | 2.02 | 232.2 | 250.6 | 218.7 | |
| Potassium standard 100 ppm | 2.56 mM | Material data sheet | 200 | | 2.41 | 2.46 | 2.45 | 2126.2 | 2795.6 | 2638.3 | 2.5 ± 0.3 mM |
| | | | 2000 | | 2.03 | 2.02 | 2.04 | 2398.0 | 2245.3 | 2656.5 | |
| Adult male mouse blood serum | 3.8 mM | [58] | 200 | | 2.47 | 2.47 | 2.44 | 2945.4 | 3137.4 | 2535.4 | 2.9 ± 0.4 mM |
| | | | 2000 | | 2.07 | 2.07 | 2.05 | 3179.4 | 3046.4 | 2796.1 | |
| Adult male mouse urine | 242 mM | [59] | 2000 | | 2.69 | 2.66 | 2.69 | 259245.3 | 178677.5 | 255165.6 | 228.7 ± 32.4 mM |
| | | | 20000 | | 2.44 | 2.40 | 2.43 | 242826.7 | 199858.6 | 236493.9 | |